Soft Matter

ARTICLE TYPE

Cite this: DOI: 10.1039/xxxxxxxxxx

Received Date
Accepted Date

DOI: 10.1039/xxxxxxxxxx

www.rsc.org/journalname

Polymers on Nanoparticles: Structure & Dynamics

Michael J. A. Hore[a]

Grafting polymers to nanoparticle surfaces influences properties from the conformation of the polymer chains to the dispersion and assembly of nanoparticles within a polymeric material. Recently, a small body of work has begun to address the question of how grafting polymers to a nanoparticle surface impacts chain dynamics, and the resulting physical properties of a material. This Review discusses recent work that characterizes the structure and dynamics of polymers that are grafted to nanoparticles and opportunities for future research. Starting from the case of a single polymer chain attached to a nanoparticle core, this Review follows the structure of the chains as grafting density increases, and how this structure slows relaxation of polymer chains and affects macroscopic material properties.

1 Introduction

Combining polymer chains with nanoparticles has led to discoveries of new types of physical behaviors, new materials, and has resulted in a rich field of active research.[1–4] When combining polymers and nanoparticles within a material, a few distinct situations arise. In the simplest case, polymers can adsorb to a nanoparticle to coat the surface. In other situations, polymers can be grafted to or from a nanoparticle surface. Grafting to a surface involves using a reactive group on the polymer chain, such as a thiol group, to bind to a complementary nanoparticle surface, such as gold. Alternatively, polymers can be grafted from a nanoparticle surface by initiating polymerization from a small molecule attached to the particle surface, such as in the case of surface-initiated atom transfer radical polymerization (SI-ATRP) or surface-initiated reversible addition-fragmentation chain-transfer polymerization (SI-RAFT).[5–8] Each technique has its relative advantages and disadvantages, and the choice of a particular technique largely depends on the characteristics of the particular system of interest as well as the desired goal, such as obtaining particles with a high grafting density of high molecular weight polymers.

Nanoparticles with polymers on the surface, both grafted and adsorbed, have been the subject of a large number of studies, and are increasingly being used in applications. Typically, the nanoparticle core imparts a functionality or physical property to a material or system. For example, Fe_3O_4 nanoparticles generate heat in response to alternating magnetic fields,[9] Au nanoparticles scatter and absorb light at particular wavelengths and polarizations,[10] and SiO_2 particles have been added to polymers to enhance the elastic modulus of the material.[11,12] Particles that form from the association of polymer chains can mimic many of the features of polymer-grafted nanoparticles. Polymer micelles are perhaps the most common example of this, in which a hydrophobic end group or block of monomers associates in the core of the micelle, leaving the hydrophilic chains to form a corona around the core. In fact, early investigations of block copolymer micelles laid the mathematical foundations used today to quantify the structure and dynamics of polymers that are attached to nanoparticle surfaces,[13] and may play a role in future studies that look at broader classes of nanoparticles, such as nanorods or nanocubes.

This Review summarizes recent progress in characterizing the structure of polymers on nanoparticle surface and their corresponding relaxation dynamics. While discussed in the context of the influence that grafted chains can have on the physical properties of a polymeric material, the primary focus of this Review is the physical behavior of the polymer chains themselves – including the structures they form, reconciling theoretical predictions with experimental measurements, and future opportunities within the field. As such, this Review is not intended to be an exhaustive discussion of polymer-grafted nanoparticle research. For the interested reader, other related Reviews in the literature examine the phase behavior and assembly of polymer-grafted nanospheres in nanocomposites,[2,3,14,15] nanocomposite dynamics,[16] polymer-grafted nanorods in polymers,[17,18] applications of such nanocomposites,[4] and other specialized topics such as single component nanocomposites (SCNCs)[1] and carbon nanotubes.[19]

[a] *Department of Macromolecular Science & Engineering, Case Western Reserve University, 10900 Euclid Avenue, Cleveland, USA. Tel: +1 216 368-0793; E-mail: hore@case.edu*

2 Structure

2.1 Mono- and Ditethered Nanoparticles

The simplest example of a polymer-grafted nanoparticle is perhaps the case of a nanoparticle that is grafted with a single polymer chain – a monotethered nanoparticle. Although they can be challenging to synthesize, some progress has been made in recent years in synthesizing such particles. One technique that has been successful is a templated approach in which reactive groups from polymers on a planar surface react with free nanoparticles in solution. Westenhoff and Kotov[20] took this approach to tether CdTe quantum dots to single poly(ethylene oxide) (PEO) chains. A similar approach from Li and Li used PEO crystals with exposed thiol groups to asymmetrically functionalize Au nanospheres.[21] The monotethered nanoparticles could be released afterwards by dissolving the crystal with sonication.

Another robust approach for synthesizing monotethered nanoparticles is to use reactive groups on polyhedral oligomeric silsesquioxanes (POSS). Work from Cheng *et al.*[22] to synthesize such particles resulted in the creation of giant surfactants, with the POSS particle behaving as a hydrophilic head group, and a grafted-to polystyrene chain behaving as a hydrophilic tail. The successful attachment of a single chain to each POSS particle was confirmed by MALDI-TOF measurements, which showed excellent agreement between the predicted mass of the product and the measured value. The particles were observed to self-assemble into micelles, vesicles, and other well-known structures. In addition, the morphology of the assembled structures was shown to be dependent on the degree of ionization of carboxylic acid groups on the POSS particle. More recently, similar approaches have resulted in analogs of gemini surfactants[23] with either POSS or C_{60} particles behaving as the head groups with two polymer tails attached. Wooley *et al.*[24] previously demonstrated attachment of two dendrimers to the surface of C_{60}. This library of mono- and ditethered nanoparticles has been shown to form ordered phases in the solid state with sub-10 nm domains, making them attractive in areas such as lithography.[23,25,26] The area of giant surfactants is a rich one, with many groups investigating a myriad of aspects concerning their assembly, uses and synthesis. Although complete discussion is beyond the scope of this Review, interested readers can find a much more complete description in recent Reviews and Perspectives on the subject.[27,28]

Polymer-grafted fullerenes, like C_{60}[24,25,29–31], are important in areas that go beyond creating ordered nanostructures or understanding their behavior as giant surfactants. For instance, grafting polymers to fullerene surfaces can enhance their solubility in organic solvents or dispersion within nanocomposites. One common approach to functionalization is cycloaddition of azide-terminated polymers with C_{60}. Kawauchi *et al.*[30] attached single isotactic poly(methyl methacrylate) (PMMA) chains to C_{60}, and imaged the particles by atomic force microscopy (AFM). The AFM images confirmed the presence of single chains, and the conformation of the PMMA chains did not appear significantly altered due to the presence of the fullerene core. Kumaki *et al.*[32] used AFM to understand the dynamics of monotethered C_{60}, and found that the particles underwent reptation-like movements on surfaces under high humidity conditions. Other polymers, such as poly(caprolactone) (PCL)[33] and poly(ethylene oxide) (PEO)[34], have been successfully grafted to C_{60} surfaces. In water, PEO-grafted C_{60} tends to aggregate due to its strong hydrophobicity, forming aggregates on the scale of 100s of nm.[34] C_{60} grafted with single PCL chains will similarly aggregate. As discussed in Section 3, the tendency for monotethered C_{60} to aggregate can significantly impact the polymer chain dynamics.

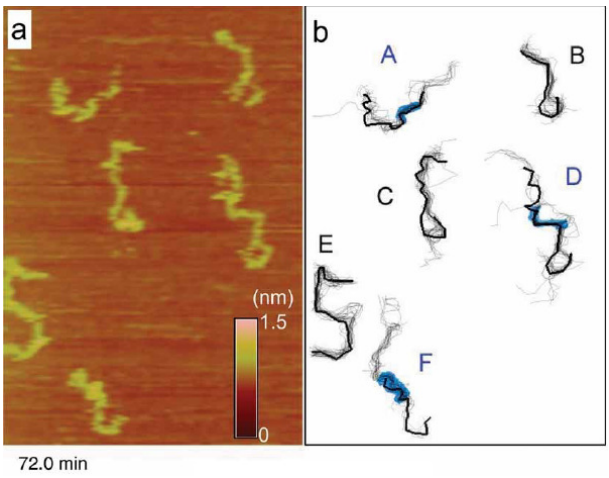

Fig. 1 Atomic force microscopy (AFM) imaging of monotethered C_{60}, showing the structure of the grafted chains. (a) AFM height image of particles after 72 minutes. (b) Time lapse image of six separate particles showing distinct conformations of the grafted polymers at separate times. The scale of the images is 300×400 nm^2. Reproduced from Ref. 30 with permission.

Alongside experimental efforts is a large body of theory and simulation using Monte Carlo, PRISM, and coarse-grained techniques (*e.g.,* Brownian dynamics) to understand phase behavior and the structure of similar monotethered nanoparticle systems. The bulk of this body of work focuses on nanoparticle assembly or aggregation into structures in solution or polymer matrices. The *structure* of the grafted polymers is largely assumed to be unaffected by the presence of the nanoparticle core, and indeed, as demonstrated by the AFM images in figure 1, this is likely a reasonable assumption. Work from the Glotzer group has used coarse-grained techniques to study monotethered nanoparticles with several geometries. Brownian dynamics simulations by Zhang *et al.*[35] investigated the role of nanoparticle shape and number of tethers on nanoparticle assembly. The geometry of the nanoparticle core (*e.g.*, sphere, rod, etc.) strongly influenced the morphology of the assembled nanoparticles, which closely resembled block copolymer morphologies. Monotethered spheres formed spherical morphologies or lamellar structures depending on the relative interaction strengths of the nanoparticle core, tether, and solvent. Monotethered rods formed lamellar structures when the tethered polymer was located at the end of the rod. Monotethered nanorods exhibited liquid crystalline phases, which have been observed experimentally in several nanorod systems.[17,36] Laterally-tethered nanorods generally assembled into side-by-side nanostructures, which transitioned between four liquid crystalline phases as temperature and par-

ticle volume fraction were varied. Interestingly, although the simulations were performed for monotethered nanorods, the resulting self-assembled structures were quite reminiscent of structures formed by polymer-grafted Au nanorods in polymer thin films.[37] Other particle shapes primarily formed cylindrical or lamellar morphologies.[38] Further investigation of monotethered, spherical nanoparticles[39] found that additional morphologies, such as perforated lamellae and hexagonally ordered cylinders, arise as the particle concentration, system temperature, and nanoparticle size are varied. In addition, Iacovella *et al.*[39] found quantitative similarities between the phase diagrams of monotethered nanoparticles and a diblock copolymer surfactant, under similar conditions. This has been observed experimentally as well by others.[28] Zhang *et al.*[40] performed systematic Brownian dynamics simulations to mimic monotethered POSS particles as a function of tether length and solvent conditions, and observed a variety of ordered structures similar to those seen in surfactant systems. Lamellar morphologies were stabilized by strong interactions between the cube-like POSS cores.

Jayaraman and Schweizer[41] applied PRISM calculations, which connect naturally with experimental scattering measurements, to understand monotethered nanoparticles under a range of conditions. PRISM calculations are advantageous in that they allow for investigation of systems at high packing fractions (up to 60%) without significant computational expense. In the absence of particle-particle interactions, particles did not exhibit strong ordering, but the potential of mean force (PMF) exhibited a transition from weak repulsion at low packing fractions to one with complex oscillations at higher packing fractions, which the authors ascribed to an interplay between depletion effects and steric repulsion. In the presence of attractions between the nanoparticle cores, strong aggregation was observed for the monotethered particles. In a separate study[42], the same authors varied the number of tethers on the nanoparticle from 1 to 4, as well as considered the effect of the location of the tethers. In general, the coordination number of the nanoparticles was observed to increase with increasing particle-particle attraction strength, and decrease as the number of tethers increased. For monotethered nanoparticles, the real space structure of the particle aggregates closely resembled that of a spherical, polymer-grafted nanoparticle (discussed in the following sections). As tethers were added to the particles, the morphology evolved from spherical to lamellar, somewhat reminiscent of similar transitions in micellar or block copolymer systems. Zhu *et al.*[43] used a combination of self-consistent field theory (SCFT) and density functional theory (DFT) to study nanoparticles with single diblock copolymer tethers. The diblock tethers underwent microphase separation, which further directed the assembly of the nanoparticles, in some cases into hierarchical structures.

2.2 Dilute and Semi-Dilute Grafting Conditions

Nanoparticles that are grafted with many polymer chains are more common in the literature than mono- or ditethered particles. Under "dilute" grafting conditions, the average distance between the graft points of neighboring chains on the nanoparticle surface is larger than their radius of gyration, i.e., $D \gtrsim R_g$, such that the conformation of the grafted chain is not significantly impacted by other chains. In describing the structure of polymers grafted under these conditions, it is convenient to compare them to symmetric star polymers. In many instances, star polymers might be considered analogous to spherical, polymer-grafted nanoparticles, since they consist of f arms grafted to a small molecule core. The question of whether the arms of a star polymer adopt ideal conformations or are stretched is at least several decades old, and a recent communication from Chremos and Douglas[44] suggests criteria to differentiate star branched polymers and polymer-grafted nanoparticles on the basis of molecular dynamics simulations. Through examination of the average segmental density of polymers as a function of f, the authors noted that star polymers with $f > 6$ behaved more like particles than linear polymers, and that beyond this threshold value of f, the arms of a star polymer will begin to be deviate from ideal chain statistics due to other grafted chains. Recent small-angle neutron scattering (SANS) measurements of poly(N-isopropylacrylamide) (PNIPAM) star polymers by Lang *et al.* observed that up to $f = 6$, the stars behaved as polymers,[45] and SANS measurements by Nickels *et al.*[46] of phytoglycogen, a highly-branched polysaccharide, showed unequivocally that those highly-branched polymers behaved as colloidal particles. SANS measurements from Richter and coworkers *et al.*[47,48] demonstrated that POSS grafted with PEO displayed behaviors similar to both star polymers and particles. As another example, the portions of chains within the corona of polymer micelles behave as unperturbed polymers at low aggregation numbers, and somewhat surprisingly, the metal junctions that comprise polymer metal organic cage (polyMOC) gels behave as though they were polymer-grafted spheres with either 4 or 24 polymer chains attached.[49,50] At such low grafting densities, where chains do not influence the conformation of neighboring chains, the polymers are said to be in the mushroom regime, and the thickness of the polymer layer is expected to scale with the degree of polymerization, N, as $H \sim N^{1/2}$ and $H \sim N^{3/5}$ in θ-solvent and good solvent conditions, respectively.[51,52] In a computational study, Binder and coworkers found that semiflexible chains exhibit different scaling relationships than flexible chains.[53] Pedersen and Schurtenberger calculated form factors to analyze such chains by scattering methods.[54] In the mushroom regime, H should be independent of the grafting density σ,[52] and the structure of polymers in the mushroom regime is not drastically different from those discussed in the previous section.

Although unaffected by neighboring chains, polymers in the mushroom regime can nevertheless adopt interesting structures, especially in poor solvent conditions. Recent work by Kumacheva *et al.*[55,56] has demonstrated the collapse of grafted polymers onto the surfaces of nanoparticles under poor solvent conditions, resulting in patchy nanoparticles. Shown in figure 2a is a schematic phase map for gold nanospheres grafted with polystyrene, at low grafting densities (σ = 0.003 to 0.2 chains/nm^2).[56] The phase map demonstrates the interplay between nanoparticle diameter (D), σ, and the number of patches (n) that form on the nanoparticle surface. At high grafting densities, where there are many chains on the surface, the polymer collapses into a uni-

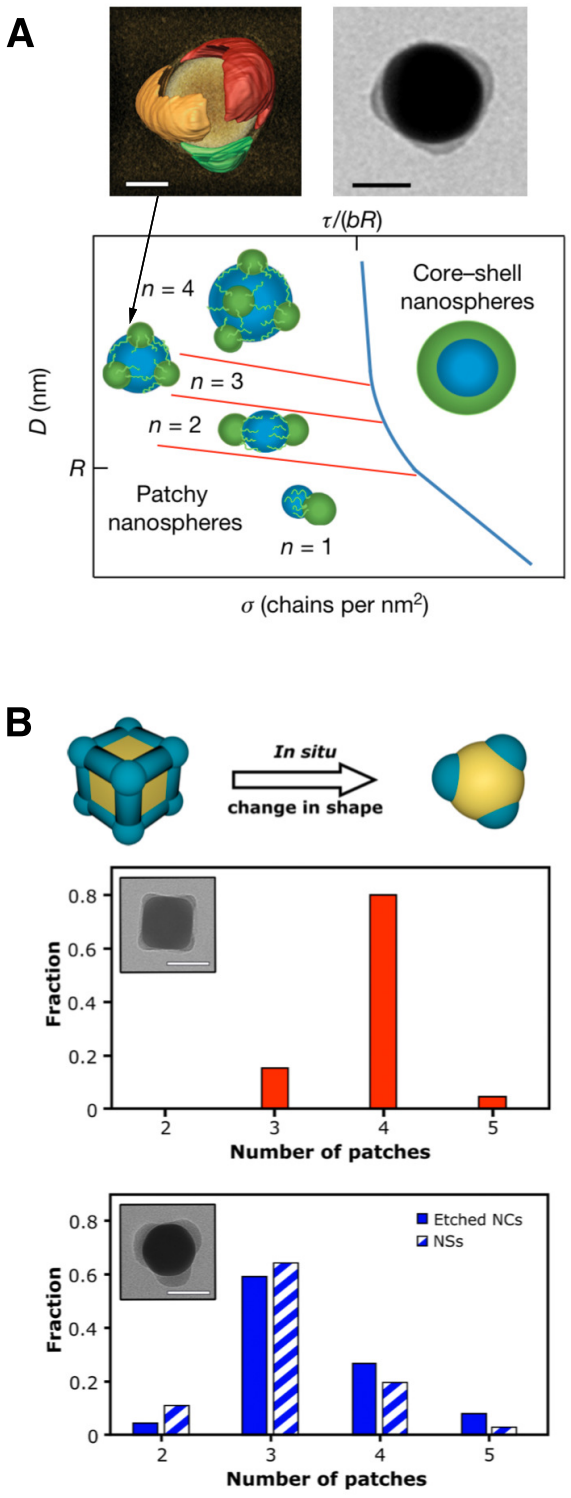

Fig. 2 (a) Schematic phase map of patchy, spherical nanoparticles as a function of grafting density, σ. The top images depict an electron tomography (left) and transmission electron microscopy (TEM) image (right) patchy particle with $n = 3$ patches. (b) The effect of nanoparticle shape on the number of patches on the particle surface. The top graph corresponds to polymer-grafted nanocubes (NCs), while the bottom graph compares etched nanocubes (solid bars) to nanospheres (dashed bars). Adapted with permission from Galati *et al.*[55]. Copyright 2017 American Chemical Society.

form shell around the particles and no patchiness is observed. However, at lower grafting densities, the phase map shows the formation of discrete patches of polymer which increase in number as D increases at fixed σ, as verified with transmission electron microscopy (TEM) and electron tomography. The shape of the nanoparticle core also influences the structures formed by the grafted polymers. Shown in figure 2b, polymer-grafted nanocubes (NCs) tend to form $n = 4$ patches for grafing densities of $\sigma \approx 0.03$ chains/nm^2 (top graph)[55], but upon etching the edges and vertices of the NCs to form a spherical core, the number of patches decreases to $n \approx 3$ (bottom graph). By comparing the etched nanoparticle (solid bars) to spherical nanoparticles (dashed bars), the authors found similar distributions of the number of patches, and concluded the geometry of the nanoparticle core strongly influences the patchiness of sparsely-grafted nanoparticles in poor solvents.

Recent theory and simulation from Asai *et al.*[57] has shown that polymer patchiness can occur in cases where the grafted polymer is not immersed in a poor solvent. Using an equivalent sphere (ES) model, and comparing results to coarse-grained simulations, the authors found that for a fixed nanoparticle size, a significant amount of the nanoparticle surface may be exposed, which is essentially independent of the degree of polymerization up to $N \approx 200$, when a single polymer chain is grafted to the surface ($f = 1$). In addition, up to 20% of the surface may be exposed for up when $f < 20$, which can be achieved at moderate grafting densities for small nanoparticle cores. Thus, patchiness may be present and may need to be accounted for in many systems, especially for those in which nanoparticles self-assemble. Jiao and Akcora[58,59] investigated the assembly of polystyrene-grafted Fe_3O_4 nanoparticles in a matrix of free polystyrene chains, using a combination of TEM, small-angle X-ray scattering (SAXS), and small-angle neutron scattering (SANS). The authors observed the formation of strings of particles over a range of low grafting densities from $\sigma = 0.02$ to 0.16 chains/nm^2.[58] String formation was attributed to dipolar interactions between the nanoparticle cores, and entanglement between the grafted polymer chains. SAXS and SANS measurements[59] found that the grafted chains were Gaussian with a size that scaled as $R \sim N^{1/2}$, indicating that the assembly of sparsely-grafted nanoparticles did not alter the structure of the grafted polymers.

Above a cutoff grafting density, the brush height becomes sensitive to the grafting density.[7,52] Early measurements by Savin *et al.*[7] showed that for $D = 10$ nm SiO_2 nanoparticles, the thickness of a grafted polystyrene layer, synthesized via atom-transfer radical polymerization (ATRP), scaled linearly with the polymer molecular weight. The Daoud-Cotton (DC) model for star polymers provides a starting point for describing the structure of polymer-grafted spheres as a function of the grafting density σ and the degree of polymerization N.[60] In the DC model, a uniform star polymer with f branches is placed into a solvent whose interactions with the star polymer are captured through the Flory-Huggins parameter χ. Ohno *et al.*[61] extended the DC model, and calculated that for a nanoparticle with radius r_{NP}, the grafted polymer chains will form a semi-dilute polymer brush if the re-

duced grafting density

$$\sigma^* = a^2\sigma \leq \left(\frac{r_{NP}}{v^*}\right)^2 \quad (1)$$

where σ^* is a reduced grafting density, σ is the "real" grafting density, v^* is an excluded volume parameter defined from the Daoud-Cotton (DC) star polymer model,[60] and a is the Kuhn length. In this regime, the thickness of the polymer layer is expected to scale as $N^{3/5}$ in a good solvent, implying that the particles prepared by Savin *et al.* were very densely grafted.

Field theoretic calculations describe the structure of grafted polymers in more detail than the DC model. Using a self-consistent field approach, Wijmans and Zhulina[62] extended calculations by Milner, Witten, and Cates to show that under good solvent conditions, polymers grafted to surfaces with low curvature (*i.e.*, a relatively large radius) form a brush layer with a thickness H which scales as

$$\left(\frac{H}{H_0}\right)^3 \left[1 + \frac{3H}{4\omega H_0} + \frac{1}{5}\left(\frac{H}{\omega H_0}\right)^2\right] = 1 \quad (2)$$

where $\omega = r_{NP}/H_0$ is a relative radius of curvature, and r_{NP} is the nanoparticle radius. H_0 describes the height of a parabolic brush profile on a flat surface as

$$H_0 = \left(\frac{8}{\pi^2}\right)^{1/3} aNv^{1/3}\sigma^{*1/3} \quad (3)$$

where N is the polymer degree of polymerization, a is the Kuhn length, $\sigma^* = a^2\sigma$ is a dimensionless grafting density, and v is the second virial coefficient. Equation 3 implies that the brush height on a planar surface scales linearly with the molecular weight of the polymers, *i.e.,* $H \sim N^1$. As the curvature of the nanoparticle surface increases, the height of the grafted polymer layer can be expressed as a scaling relationship

$$H \sim \left(N^3 r_{NP}^2 \sigma v\right)^{1/5} \quad (4)$$

which clearly shows the $N^{3/5}$ scaling of the brush height expected for polymer chains in a good solvent, in accordance with the extended DC model. This scaling relationship is expected to emerge at distances far away from the nanoparticle surface, where the curvature is much lower, and there are no influences from neighboring chains due to the lower concentration (*e.g.*, in high molecular weight samples).

The use of equation 2 (*i.e.*, the MWC-WZ model) for the thickness of the polymer layer has been validated experimentally. Most recently, work from the Vaia group[63] used dynamic light scattering (DLS) to determine the brush height as a function of molecular weight, demonstrating excellent agreement between the thickness estimated from the hydrodynamic radius and estimates using equation 2, as shown in figure 3a. An important feature observed in this data is the $N^{0.65}$ scaling of the brush height with molecular weight (*i.e.*, N), indicating that the brush is slightly extended as compared to free chains in solution. This scaling relationship is very close to that predicted by Hore *et al.*[64] using SCFT for similar particles, shown in figure 3b, which found that for grafted

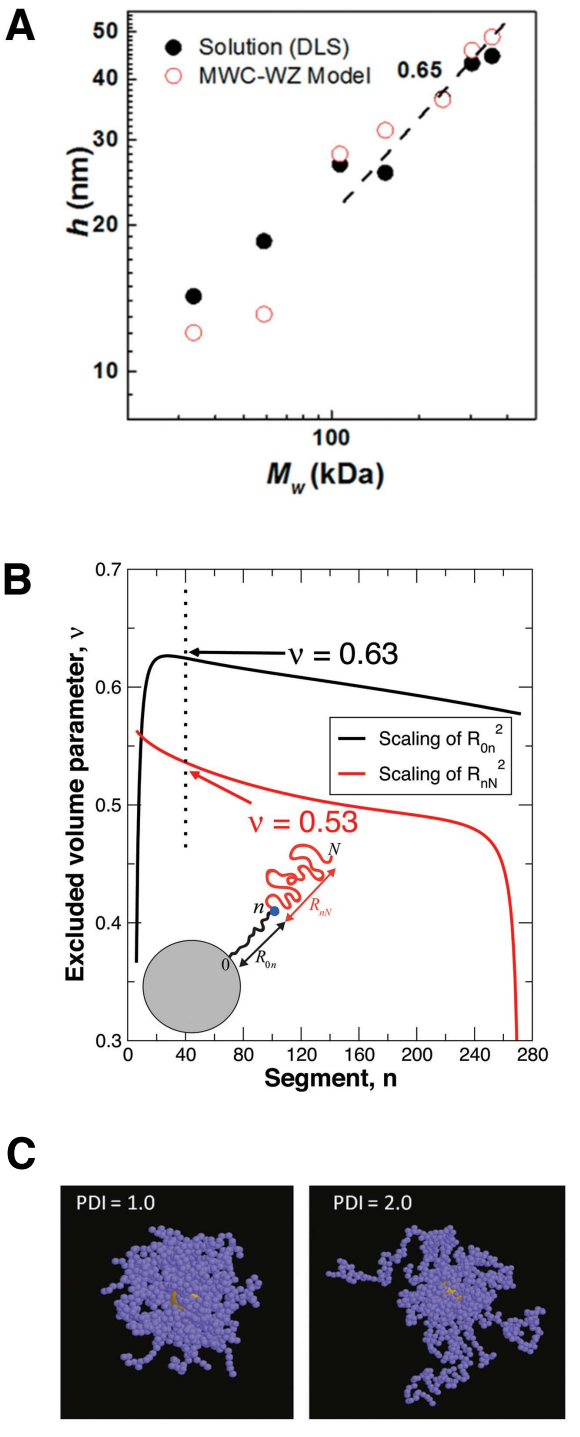

Fig. 3 (a) Dynamic light scattering (DLS) measurements (solid points) of the hydrodynamic thickness of the brush, h, as a function of molecular weight. Shown as open symbols are estimates of the brush thickness according to equation 2. Reproduced with permission from Jiao *et al.*[63]. Copyright 2018 American Chemical Society. (b) Estimates from self-consistent field theory (SCFT) calculations of the scaling exponents for the brush height of polymer-grafted as a function of the number of Kuhn segments. R_{0n} is the height of the brush from the surface of the nanoparticle. R_{nN} is the scaling of the outer portion of the brush. Reproduced with permission from Hore *et al.*[64]. Copyright 2013 American Chemical Society. (c) Visualization of the effect of polydispersity (PDI) on polymer conformation from Monte Carlo simulations. Dodd and Jayaraman[65]. Copyright 2012 Wiley Periodicals, Inc.

polymers with less than approximately 40 Kuhn segments, the height of the brush scaled as $N^{0.63}$, although at slightly different grafting densities. For the polystyrene-grafted nanoparticles studied by Jiao *et al.*[63], this corresponds to molecular weights of less than approximately 28 kg/mol[51]. Monte Carlo simulations by Dodd and Jayaraman[65] also found scaling exponents of $\nu \approx 0.65$ for $0.1 \leq \sigma^* \leq 0.65$. For monodisperse chains at $\sigma^* = 0.65$, the authors found $H \sim N^{0.65}$, in good agreement with measurements and theory. As the polydispersity increased from $Đ = 1.0$ to 2.5, the scaling exponent decreased slightly to $\nu = 0.63$. The effect of the dispersity can be observed using snapshots from Monte Carlo simulations, shown in figure 3c, in which the polydisperse system shows long chains protruding from the grafted layer, where they do no appear strongly influenced by the presence of other chains. For comparison to experimental studies, most grafted polymers synthesized by surface-initiated controlled radical polymerization schemes have $Đ < 1.3$.[7,61,63,64].

2.3 High Grafting Conditions

The structure of grafted polymers becomes most complex at high grafting densities. At high grafting densities, the extended DC model predicts two regions of polymer concentration: a concentrated polymer brush (CPB) near the nanoparticle core and a semi-dilute polymer brush (SDPB) farther away. The cutoff distance between these two regions can be estimated from the extended DC model, and is given as:

$$r_c = r_{NP} \frac{\sqrt{\sigma^*}}{\nu^*} \tag{5}$$

where $\sigma^* = a^2\sigma$ is a dimensionless grafting density, r_{NP} is the nanoparticle core radius, and the excluded volume $\nu^* = (4\pi)^{-1/2}(1/2 - \chi)$. χ is the Flory-Huggins parameter between the grafted chains and their matrix. At high grafting densities and large molecular weights, the chains may be fully stretched.[66]

Several groups have measured the thickness of the grafted polymer layer using a variety of techniques, including DLS,[61,63,66,67] electron microscopy,[68] and small-angle neutron scattering (SANS).[64,69–73] The general structure of the brush at high grafting densities is shown in figure 4. DLS measurements by Ohno *et al.*[61] and Dukes *et al.*[67] as a function of molecular weight showed two distinct scaling relationships as molecular weight increased. Ohno *et al.* found the thickness of the CPB region scaled as $H \sim N^{0.83}$ for poly(methyl methacrylate) (PMMA) in acetone whereas Dukes *et al.* found $H \sim N^{0.7}$ for polystyrene in benzene. When plotted together, Dukes and coworkers found remarkable agreement between the scaling exponent observed in their measurements, as well as those by Ohno *et al.*[61] and Savin *et al.*[7]. It is worth noting the limitations of both the DC and MWC-WZ models to describe grafted polymers, as pointed out in the work of Dukes *et al.*[67] Although the MWC-WZ model predicts that the height of the CPB region should scale linearly with N, as in the case of a planar brush, measurements have consistently found $H \sim N^{3/4}$. Similarly, the extended DC model predicts that the thickness of the CPB region scales as $H \sim N$. Monte Carlo simulations by Laradji for planar, flexible, polymer-grafted membranes are able to recover the $N^{3/4}$ scaling, indicating that this value likely arises due to curvature effects.[74] As shown in figure 3, the MWC-WZ model correctly describes the brush height for large molecular weights where the effect of the CPB region may be relatively small. Another limitation of the DC model is that it treats the change in conformation between the CPB and SDPB regions as a step function, when in reality, the transition is likely gradual.[75] As noted by the authors of several studies[12,67] of the CPB region, because both the extended DC and MWC-WZ models consider only pairwise interactions, their ability to correctly describe confinement in the CPB region or more complex systems are limited. Nevertheless, both models are extremely useful in providing a general picture of polymer conformation. The extended DC model is noteworthy in its simple prediction of the size of the CPB region (*cf.* equation 5), which has been recently verified by SANS measurements.[64,69]

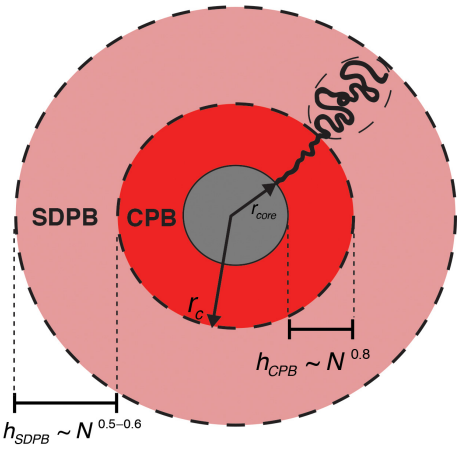

Fig. 4 Structure of grafted polymer chains at high grafting densities in the CPB and SDPB regions. The scaling of the brush heights h are noted in each region. Reprinted from Lenart and Hore[4], copyright 2017, with permission from Elsevier.

Goel *et al.*[76] combined several techniques – SAXS, SANS, TEM, rheometry – to examine both structure and dynamics in poly(*n*-butyl acrylate) (PBA) or poly(syrene-*co*-acrylonitrile) (PSAN)-grafted SiO_2 nanoparticles. While the interparticle spacing between nanoparticles scaled as $N^{1/2}$, when the spacing was compared to the dimensions of ungrafted chains with similar molecular weights, the authors observed that the chains must be stretched by at least a factor of two. Thus, the combination of scattering and microscopy can reveal structural information that may be difficult to obtain using either technique alone.

The availability of suitable scattering models is necessary for fully characterizing the structure of grafted polymers.[13,47,48,54,64,69,77] Within the past five years, advances in scattering models have led to the ability to directly access scaling exponents of the CPB and SDPB regions without the need for preparing a series of molecular weights. This is important as it allows researchers to fully characterize the brush of a single grafted-nanoparticle system, and understand how its structure influences other physical properties. Central to these developments is the use of the form factor $P_p(q)$ and form factor amplitude $F_p(q)$

for a polymer with excluded volume:

$$P_p(q) = \frac{1}{\nu U^{1/2\nu}}\gamma\left(\frac{1}{2\nu},U\right) - \frac{1}{\nu U^{1/\nu}}\gamma\left(\frac{1}{\nu},U\right) \quad (6)$$

$$F_p(q) = \frac{1}{2\nu U^{1/2\nu}}\gamma\left(\frac{1}{2\nu},U\right) \quad (7)$$

where $\gamma(x,y)$ is the lower incomplete gamma function, $q = (4\pi/\lambda)\sin(\theta/2)$ is the scattering vector, and $U = q^2a^2N^{2\nu}/6$. Whereas the Debye function *only* describes scattering from polymer chains with $\nu = 1/2$, these functions are able to capture scattering for $\nu = 1/3$ (globule) to $\nu \approx 1$ (extended chain). SANS measurements by Hore *et al.*[64] incorporated these functions into a core-shell-chain (CSC) form factor to characterize the structure of PMMA-grafted Fe_3O_4 nanoparticles ($r_{NP} = 2.5$ nm). The CSC model describes polymer-grafted nanoparticles as a spherically symmetric core, surrounded by a shell of polymer with uniform density, which is grafted with N_c chains a distance r_c away with an excluded volume parameter ν. Using this model, the authors were able to confirm the accuracy of the extended DC model in predicting r_c, as well as in confirming that the SDPB size should scale as $H \sim N^{1/2}$ when $\chi = 0$. This model has been used to characterize the junctions in polyMOC gels[49], and can be extended to estimate the number of primary loops at those junctions.[50] In the limit that the shell thickness $t \to 0$, the model can describe scattering from spheres with low grafting densities (*i.e.*, particles with mushrooms or a SDPB region only). Of course, other scattering models can be successfully applied as well. Mark *et al.*[78] studied polyisoprene (PI)-grafted SiO_2 nanoparticles with SANS. Using a spherical core-shell model with terms to describe the conformation of the grafted polymers, the authors were able to capture both the structure of the particles, as well as the decay in the density of the corona, finding a profile that scales with distance as r^{-1}, in agreement with predictions from the DC model.[60,78]

The combination of X-ray and neutron scattering[70–72,76,79] has helped to simultaneously elucidate the behavior of nanoparticles and polymers grafted to their surface, respectively, inside of polymer nanocomposites. Neutron scattering, in particular, is useful for characterizing grafted polymers because of its isotopic sensitivity, especially between hydrogen and deuterium. Recent work by Wei *et al.*[69] extended the CSC model to explicitly account for the conformation of the CPB region. The authors measured poly(methyl acrylate) (PMA)-grafted SiO_2 nanoparticles with SANS, and fit the results to a core-chain-chain (CCC) model. Regions of interest, such as the CPB region, were composed of fully hydrogenated PMA. To suppress scattering from other regions of the sample, Wei *et al.* took advtange of natural contrast match conditions between SiO_2, partially deuterated poly(methyl acrylate-d_3), and the solvent (1,1,2,2-tetrachloroethane-d_2). The result was that measurements were performed on poly(methyl acrylate)-b-poly(methyl acrylate-d_3)-grafted SiO_2 to characterize the CPB region, and on poly(methyl acrylate-d_3)-b-poly(methyl acrylate)-grafted SiO_2 to characterize the SDPB region. The authors found the thickness of the CPB region scaled as $H \sim N^{0.8}$, and that the SDPB region thickness scaled as $H \sim N^{3/5}$, as expected for polymers in a good solvent. However, the scaling relationships represented the average scaling exponents across the respective regions, and the measurements were not sensitive enough to observe a gradual transition in conformation as the distance from the nanoparticle core increased. Regardless, the measurements further confirmed the estimate for r_c given by the extended DC model and showed directly that the CPB region is highly stretched for high grafting density, high molecular weight samples.

From a practical standpoint, the grafting density strongly influences the physical properties of materials made from polymer-grafted nanoparticles due to the effect it has on the structure of the grafted chains. For example, Gao *et al.*[11] systematically varied the grafting density of poly(hexyl methacrylate)-b-poly(glycidyl methacrylate) on SiO_2 nanoparticles and investigated the effect that this had on the mechanical properties of epoxy nanocomposites, including elastic moduli and fracture properties. Lower values of σ improved the fracture toughness. Work from Bockstaller's group[12,80] studied densely grafted particles (discussed in the next section) as a function of molecular weight. Their measurements provide insight into the origin of the mechanical enhancements observed in grafted particle systems, as they show the largest enhancement at high molecular weights. Crazing was observed at these conditions, whereas at lower molecular weights or high σ, the nanocomposites were fragile. At high molecular weights, the conformation of the chains is more ideal, as implied by equation 4, and the chains have greater opportunities for entanglement, leading to this behavior. Interestingly, fragile composites were observed in instances where the molecular weight of the grafted polymers was above the entanglement molecular weight, highlighting the importance of the structure of the grafted polymer layer. Highly stretched polymer chains result in a lower amount of entanglement, and more fragile composites. Jiao *et al.*[63] found a similar behavior for polystyrene-grafted Fe_3O_4 nanoparticles, finding that crazing occurred only when a semi-dilute polymer brush was present on grafted nanoparticles. Recent calculations from Asai *et al.*[81] observe similar behavior. Koerner *et al.*[82] investigated how grafted chain conformation affects the assembly of particles in single component nanocomposites (SCNCs) using X-ray scattering, finding that the brush characteristics can lead to anisotropic assembly of the nanoparticles. Specifically, whereas SCNCs composed of nanoparticles with a grafting density of $\sigma = 0.05$ chains/nm^2 formed grains of aligned strings, the morphology was completely isotropic when the grafting density increased to $\sigma = 0.1$ chains/nm^2. Upon deformation, the grains of strings for the lower grafting density sample aligned in the direction of applied stress, but the high grafting density sample was characterized by the formation of chevron structures rather than aligned strings. The authors attributed this difference in morphology to a difference in the initial strain distribution in the material, highlighting the fact that while the mechanical properties of both materials may be similar, the internal morphology and strain distribution can be distinct as a result of brush conformation.

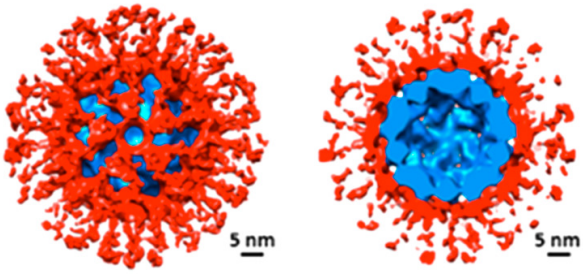

Fig. 5 Cryo-EM reconstruction of a Qβ virus-like particle (blue) grafted with poly(norbornene-oligo(ethylene glycol) ester) (PNB) (red). Shown in the cross-sectional image on the right, the PNB polymer forms a thin shell on the Qβ surface, decorated with small globules. Adapted from Lee *et al.*[83]. Copyright 2017 American Chemical Society.

2.4 Influence of Chemistry and Polymer Architecture

An underlying assumption in both the extended DC model and the MWC-WZ model is that the grafted polymers are linear, and that only pairwise interactions occur. Of course, in many polymer systems, neither of these assumptions may be true, and may result in drastically different structures than would be inferred from either of these models. Monte Carlo simulations, for example, have shown that for grafted copolymers, the monomer sequence and monomer-monomer interaction strengths can alter the scaling of the radius of gyration of the chains.[84] The authors observed patchy structures, globular structures ($\nu \approx 0.3$), swollen chains ($\nu \approx 0.6$), and even highly stretched chains ($\nu \approx 0.8$) in the case of athermal systems at high grafting densities.

One example of the effect of chain interactions can be seen in the recent work of Lee *et al.* ,[83] who grafted a poly(norbornene)-like polymer (PNB) to the surface of Qβ virus-like particles (VLPs). The authors of this study used cryogenic electron microscopy (cryo-EM), shown in figure 5, and SANS to determine the structures of the grafted polymers. As shown in the figure, PNB forms a complex structure consisting of a thick shell of polymer on the Qβ surface, with protruding PNB globules (red region). SANS from the free homopolymers in D_2O indicated that the free polymer formed globules in solution, despite being highly soluble, and that this structure persisted when the chains were grafted to the VLP surfaces. Measurements from Kim and Archer[85] have shown that PEO chains can form helical structures when grafted to SiO_2 nanoparticles at high grafting densities. Neither the extended DC or MWC-WZ models predict or capture this behavior, although analysis of scattering within a framework such as the CSC or CCC model may yield valuable information in both cases. Martin *et al.*[86] combined coarse-grained molecular modeling with SANS to investigate the wetting-dewetting transition of polymer-grafted nanoparticles in a chemically dissimilar matrix with LCST behavior. The Brownian dynamics simulations captured many of the trends observed in SANS measurements, highlighting the power of combining scattering with complementary techniques to understand complex systems.

In some instances, polymers may collapse despite favorable interactions between the monomers and solvent molecules, such as when the Flory-Huggins parameter χ is concentration dependent. N-clustering is an n-body interaction,[87] which is not captured by the extended DC or MWC-WZ models. This is the case for PNIPAM, and "n-clustering" can lead to departures from the structures that would expected in the context of a framework like the extended DC model. N-clustering is also observed for poly(ethylene oxide).[88,89] Shan *et al.* attached thiol-terminated PNIPAM to Au nanospheres, and observed the presence of two conformational transitions: one at its aqueous lower critical solution temperature (LCST) of $T_C = 32$ °C, and another near 20 °C. The authors attributed the transition at $T = 20$ °C, which is not observed for free chains in solution, to collapse of the grafted chains due to strong interactions between one another. Thus, the structure of grafted PNIPAM at $T > 20$ °C consists of a collapsed shell of polymer near the polymer core, with a dilute collection of chain ends protruding from the surface farther away. This is not unlike what was observed by Seifpour *et al.*[84] in Monte Carlo simulations, although the PNIPAM homopolymer is considerably more simple than a copolymer. Lang *et al.*[90] observed a similar structure in micelles formed from a set of related poly(N-alkyl acrylamide) polymers that were terminated with a dodecyl group. The scaling exponent of the portion of the chain within the corona of the micelle was lower than that of a free chain, implying that the presence of neighboring chains within the micelle lead to a more collapsed conformation due to n-clustering.

As in the case of polymer micelles, other self assembled structures may exhibit many of the characteristics of grafted polymer chains, such as in the case of particles formed from polymerization-induced self-assembly (PISA) or the polyMOC gels discussed above.[91,92] PISA particles can be formed by chain extending a hydrophilic macro-chain transfer agent (macro-CTA) with a hydrophobic block using RAFT. The copolymer concentration and degree of polymerization of the blocks control the self-assembly into spherical, worm-like, or vesicle morphologies. SAXS measurements of spherical and worm-like particles produced from PISA distinctly showed a decay in the scattering intensity at high q that is consistent with a polymer corona similar to that found on grafted nanoparticles. Separate SAXS measurements[93] of PISA vesicles yielded the radius of gyration (R_g) of the corona of the vesicles as well as the aggregation number. However, no attempt was made to extract the conformation of the corona from the SAXS spectra, for example, with more detailed form factors[64,69]. To the best of the author's knowledge, while there has not yet been observation of CPB and SDPB-type regions for particles formed by PISA, the DC model predicts that the regions can emerge given sufficient concentrations of chains in the corona.[60,61] One difference between PISA particles and inorganic nanoparticles is that the core size for a given morphology (*e.g.*, vesicles) may not be as tunable. For instance, DLS measurements of PISA particles[94] show that the size of spherical PISA particles can be varied between 40 and 100 nm by increasing the degree of polymerization of the hydrophobic core from 250 to 1000. Vesicles had much larger diameters on the order of 200 nm. Thus, for a given morphology, it may be difficult to tune the conformation of the corona due to a strong interplay between aggregation number and particle size, with larger particles leading to more stretched coronas (*cf* equation 5).

SANS measurements of polystyrene-grafted SiO_2 nanoparticles have shown that grafting a chain to a nanoparticle surface can alter interactions between it and its environment. Mongcopa *et al.*[95] found the θ-temperature of the polystyrene/cyclohexane-d_{12} system was depressed from $T_\theta = 38$ °C for free chains to $T_\theta = 34$ °C for grafted polystyrene. The authors suggested a change between the balance of entropic and enthalpic forces for grafted chains resulted in the shift, further suggesting additional measurements to definitively determine the origin. Because the polymer chain conformation is directly related to the enthalpic and entropic forces a grafted chain experiences, future theoretical treatments of grafted chain structure may need to take these differences into account. SANS measurements by Buenning *et al.*[73] suggest that for SCNCs, swollen with ethyl acetate, made from PMA-grafted SiO_2 nanoparticles, the Daoud-Cotton model may no apply, motivating the need for additional investigations into such systems.

Recently, the effect of polymer molecular weight dispersity on brush structure has been receiving increasing attention, especially in the case of bimodal molecular weight distributions.[96–98] Bimodal brushes can be synthesized via two successive RAFT polymerizations[96] or by SI-ATRP[99], and have been shown to broaden the range over which nanoparticles can be dispersed within a polymer matrix[96,97]. Bimodal brushes also enhanced the mechanical properties of polymer nanocomposites.[97] In the case of SCNCs, bimodal brushes can be used to simultaneously reinforce a material mechanically while maintaining excellent dispersion of the nanoparticles. One area in which this is important is in high refractive index SCNCs.[98] As demonstrated in a recent experimentally-validated, computational study, polydispersity in the brush is central to the morphology of nanoparticle self-assemblies.[100]

Limited studies have begun to consider the effect of non-linear architectures on the structure of grafted polymers. Modica *et al.*[101] used Langevin dynamics simulations and PRISM theory to investigate the effect of side chains on the conformation of grafted comb polymers. With increasing numbers of side chains and increasing grafting density, the backbone became increasingly stretched, with $R \sim N^{0.8}$ for the shortest side chain length at the highest grafting density ($\sigma^* = 0.65$). As the side chain length increased, and grafting density decreased, $\nu \to 0.7$. Future measurements of grafted bottlebrushes or poly(norbornene)-derived polymers may be interesting complementary studies to these simulations.

3 Dynamics

Compared to what is known of the conformation/structure of grafted chains on particles, a relatively small amount is known of their relaxation dynamics. Work from several groups within the last decade is shedding light on the effect that grafting has on polymer relaxation and resulting macroscopic material properties.[85,102–105,105–110] For instance, grafting polymers to a nanoparticle surface can affect the timescales over which the chains relax. Changes in the relaxation of polymer chains can impact mechanical properties, such as the loss and storage modulus, and affect stress relaxation. Dielectric spectroscopy measurements of polyisoprene (PI)/clay nanocomposites by Mijović *et al.*[110] found that for high molecular weight PI, increasing clay content within a nanocomposite led to suppression of long-time relaxation modes and an increase in the relaxation time of the normal mode, which they attributed to confinement effects. Macroscopically, this was correlated to an increase in the storage modulus of the composites as the clay content increased. However, measurements of chain relaxation in C_{60}-containing nanocomposites found the addition of C_{60} had an insignificant effect on the normal mode relaxation times, and that segmental relaxation modes were affected most, highlighting how different nanoparticles may affect systems differently at different length scales. As discussed in the previous section, the process of grafting a polymer chain to a nanoparticle surface can result in confinement, whether by restricting the diffusion of the chain by anchoring it to a nanoparticle, or by spatially confining it because of the presence of neighboring chains. Because of this, it is reasonable to expect that grafted chains may exhibit different dynamics than free chains, and perhaps at different length scales.

For monotethered, PMMA-grafted C_{60}, time-lapse AFM imaging was able to capture the dynamics of the chains on mica surfaces (*cf.* figure 1).[32] The authors of the study observed a unique reptation-like movement of the chains in which they moved forward and backward from the C_{60} particle along the same path. The authors inferred that the combination of the mica substrate and adsorbed water may have been the primary factors that influenced the motions of the chains. In composites synthesized from PCL-grafted C_{60}, aggregation of the C_{60} was associated with a decrease in the PCL mobility which affected both the glass transition temperature and the crystallinity of the PCL.The behavior of PCL-grafted C_{60} upon aggregation is somewhat similar to the relaxation dynamics observed in other nanocomposites.

Neutron spin echo (NSE) spectroscopy is currently able to access the largest window of time and length scales for polymer systems.[111] Schneider *et al.*[112] used NSE to measure the dynamics of the polymer matrix in nanocomposites containing polyisoprene-coated SiO_2 nanoparticles within a poly(ethylene-propylene) (PEP) matrix. Although the decay in the intermediate structure factor (ISF), $I(q,t)/I(q,0)$, was decreased by increasing the particle concentration, the authors found that the PEP chains retained Gaussian conformations. Furthermore, while the overall ISF varied with nanoparticle concentration, the initial decay of the ISF was described well by the Rouse model for unconfined polymers. The authors concluded that the local dynamics of the polymers were unchanged, and increasing the particle concentration resulted in tube diameters that decreased with increasing particle concentration. Thus, the difference between the dynamics in filled and unfilled materials was due to differences in entanglement.[112] X-ray photon correlation spectroscopy (XPCS) measurements of PMMA-grafted Au nanoparticles dispersed in PMMA homopolymer[113] showed that changes in polymer dynamics at small length scales influence nanoparticle dynamics, as well. Freilinghaus *et al.*[114] combined SANS and neutron spin echo (NSE) to measure the structure and collective dynamics, respectively, of Laponite/PEO nanocomposites. The NSE spectra that were collected for the Laponite/PEO system were described

by a fast decay over 10 to 20 ns, followed by a plateau that did not decay to zero. The authors ascribed this behavior to the presence of regions of PEO that were immobilized on the Laponite surfaces, significantly restricting their relaxations. More recent NSE measurements of carbon black (CB)/polybutadiene nanocomposites have measured the collective dynamics of polymer chains in the presence of particles, and clarified the role of nanoparticles in slowing chain dynamics. In their work, Jiang *et al.*[115] found many similarities with the measurements from Freilinghaus *et al.* , including the presence of a fraction of immobilized polymer on the nanoparticle surface. However, their detailed analysis of the NSE spectra discovered evidence of "breathing modes" in the portions of the polybutadiene that was not immobilized by the carbon black. Breathing modes are characterized by a quick decay of the normalized ISF, followed by a long-time plateau.[116] Physically, breathing modes correspond to collective, longitudinal motions along the direction of the polymer contour.[117]

Given that nanoparticles appear to slow or stop the relaxation of polymers that adsorb to their surface, a natural question to ask is how the actual dynamics of grafted chains differ from those that are untethered or adsorbed. Holt *et al.*[105] explicitly investigated the difference between grafted and adsorbed chains using broadband dielectric spectroscopy (BDS), finding that the chain stretching that occurs near the nanoparticle surface results in slowing of segmental dynamics. Recent work from Archer and coworkers has used also employed BDS to extensively investigate the relaxation dynamics of PI-grafted nanoparticles to help address this question.[102–104,118] BDS measurements found that the normal mode relaxation time (τ) increased as σ increased due to increasing confinement by neighboring chains.[102] As molecular weight increased, untethered chains showed a larger variation in their relaxation times than grafted chains. In another study,[104] rheological measurements showed that the grafting density influences the storage and loss moduli of nanocomposites containing PI-grafted SiO_2 particles. Composites containing moderately-grafted nanoparticles ($\sigma = 1.21$ chains/nm^2) had higher elastic moduli, over a wider frequency range, than composites containing densely-grafted particles ($\sigma = 1.68$ chains/nm^2) due to increased entanglement/interpenetration between the brush layers at lower grafting densities.Recent simulations from Ethier and Hall[119] support this finding. BDS measurements as a function of grafted chain molecular weight found that grafted chains, in general, showed increased relaxation times relative to free chains. The difference between the relaxation times of grafted and free chains decreased as the molecular weight of the polymer increased, as shown in figure 6a. This finding can be rationalized by considering the structure of a grafted chain. At low molecular weights and high grafting density, a polymer chain is expected to be highly stretched relative to a free chain. This difference decreases as the molecular weight of the polymer increases, and a larger amount of the chain resides in the SDPB region of the brush. When the effect of grafting density was considered, low molecular weight PI chains relaxed more slowly at moderate grafting densities ($\sigma = 0.64$ and 1.21 chains/nm^2) than at the highest grafting density ($\sigma = 1.68$ chains/nm^2), as shown in figure 6b. This behavior might be attributed to increased entanglement of the grafted polymers with the matrix at lower grafting densities. Holt and coworkers[120] compared segmental dynamics in traditional polymer nanocomposites consisting of SiO_2 nanoparticles dispersed in poly(2-vinyl pyridine) homopolymer (P2VP) to P2VP grafted SiO_2 nanoparticles. Their results showed that local dynamics are affected primarily by chain density, but the mechanical properties of the materials were affected by polymer conformation and density. Thus, grafting a polymer to a surface may slow local dynamics because of the high concentration of chains on the nanoparticle surface. The high density of *grafted* chains leads to chain stretching, however, which in turn affects properties such as the modulus of the material.

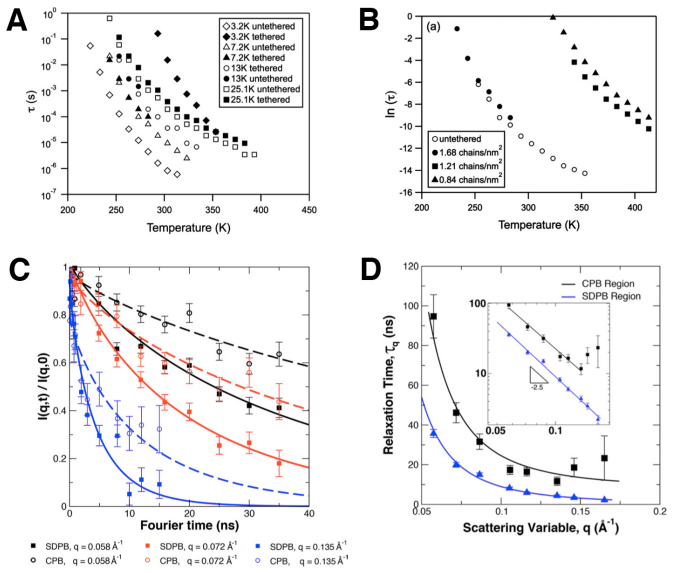

Fig. 6 Dynamics of grafted polymers. (a) Relaxation times for grafted (solid symbols) and ungrafted (open symbols) polyisoprene (PI) at several molecular weights. (b) Relaxation times for 7.2 kg/mol PI as a function of temperature for several grafting densities. (c) Neutron spin echo measurements of the CPB (dashed lines) and SDPB (solid lines) regions of a grafted poly(methyl acrylate) brush. (d) Relaxation times for the CPB (black) and SDPB (blue) regions. The inset shows a double logarithmic plot confirming Zimm-like behavior. (a-b) Reproduced with permission from Kim *et al.*[104]. Copyright 2015 American Chemical Society. (c-d) Reproduced with permission from Wei *et al.*[69]. Copyright 2018 American Chemical Society.

NSE measurements are able to probe the relaxation dynamics at different length scales, and can take advantage of isotopic sensitivity to explicitly probe the structure and dynamics of local regions of a grafted polymer chain. For this reason, they are an incredibly powerful means of assessing polymer dynamics in grafted systems. NSE measurements by Poling-Skutvik *et al.*[121] investigated how relaxation dynamics of grafted polymers are affected by the presence of untethered chains. The authors analyzed their results in terms of a modified Kohlrausch-Williams-Watts (KWW) function:

$$\frac{I(q,t)}{I(q,0)} = (1-f)\exp\left[-\left(\frac{t}{\tau}\right)^{\beta}\right] + f \qquad (8)$$

where f is the fraction of chains that are immobile, τ is a char-

acteristic relaxation time at scattering vector q, and β is a parameter which yields information on the relaxation. For unentangled dynamics in the absence of hydrodynamic effects, $\beta = 0.50$ (Rouse dynamics). When hydrodynamic effects play a major role, $\beta \approx 0.85$ (Zimm dynamics). Richter *et al.*[111] provide a detailed discussion of the origin of these expressions, noting that $\beta \approx 0.85$ is an approximation common to NSE. Analysis according to equation 8 found that Zimm dynamics were dominant at short time scales, but over long times, little relaxation occurred. Breathing modes were not observed.

For the PMA-grafted SiO_2 particles studied by Wei *et al.* ,[69] partially deuterating the SDPB region of the brush, and leaving the CPB fully hydrogenated, allowed the authors to directly measure the relaxation dynamics of the CPB region due to contrast matching. The dynamics of the SDPB region could be directly measured by reversing the deuteration scheme. The authors analyzed NSE results in terms of equation 8, with $f = 0$. The dynamics of both the CPB and SDPB regions were described well by Zimm dynamics ($\beta = 0.85$) at all length scales, as confirmed in figure 6c. However, the relaxation times of the CPB region were approximately three times longer than that of the SDPB (figure 6d). It is not clear why Zimm dynamics were observed in both regions of the brush since the polymer concentration is assumed to be much higher near the nanoparticle surface. SANS measurements by Buenning *et al.*[73] observed that solvent readily penetrates both regions at high concentrations, providing a possible explanation. As in the work from Poling-Skutvik, no breathing modes were observed in this system.

Although experimental studies of the dynamics in polymer-grafted nanoparticle systems are just emerging within the last several years, there is a relative wealth of theoretical and computational work available that can guide future research. Molecular dynamics (MD) from Binder and coworkers have examined dynamics in polymer brushes under a range of conditions. In one study, Reith *et al.*[122] determined the relaxation times for planar grafted polymers as a function of position along the contour, finding a maximum in τ at positions deep within the brush. When simulations were extended to spherical surfaces, the general trend of increased relaxation times at intermediate positions along the polymer contour was still observed.[123] An interesting aspect of simulations of spherical nanoparticles was that the increase in τ at intermediate contour positions was amplified as the nanoparticle radius was increased (*i.e.* the curvature decreased). Chremos *et al.*[124] examined the dynamics of nanoparticles, polymer-grafted nanoparticles in a polymer matrix, and SCNCs using MD. In the absence of solvent, the authors found that the grafted polymers play the largest role in the dynamics. Short grafted chains do not significantly alter the nanoparticle dynamics compared to hard nanoparticles, whereas long grafted chains lead to melt-like dynamics of particles that behave as hyperbranched polymers. For long polymer chains, a natural question that arises is what role grafting plays on entanglements, which can significantly affect relaxation dynamics. Simulations by Hoy and Grest[125] investigated entanglements of planar grafted polymers in polymer melts and solvents by primitive path analysis. In solvents, the number of entanglements in the brush increased as the solvent quality decreased. In polymer melts, entanglements in the brush increased as grafting density increased. Work from Kalb *et al.*[126] is in agreement, implying that in the case of spherical, polymer-grafted nanoparticles, one might expect a greater degree of entanglement in the CPB region than in the SDPB region, where the monomer concentration is much lower. An experimental measurement of such an effect would be a great opportunity to increase our knowledge of such systems. Entanglements between polymers grafted on nanoparticles and free chains in a polymer matrix have been shown to lead to subdiffusive motions of nanoparticles.[47]

Interestingly, interactions between nanoparticles can also affect relaxation dynamics. In another study, Agrawal *et al.*[118] blended PMMA-grafted SiO_2 with PEO-grafted SiO_2. PEO and PMMA interact favorably with each other.[127] As the volume fraction of PMMA-grafted particles (ϕ_{PMMA}) increased, SAXS measurements of the interparticle structure factor showed the interparticle separation decreased monotonically until $\phi_{PMMA} \approx 0.5$, after which it increased to its initial value at $\phi_{PMMA} = 1.0$. The decreased particle separation was attributed to favorable interactions between PMMA-grafted particles and particles grafted with PEO – resulting in increasing interpenetration between the brushes of the two components. Associated with the decrease in particle separation was an increase in the relaxation time of the grafted polymers. When compared to free chains, grafted chains showed the largest increase in relaxation time for the value of ϕ_{PMMA} which showed the smallest interparticle separation. Better space filling of the polymer brushes at this value of ϕ_{PMMA} led to increased confinement of the polymers, and slower relaxation of the chains. As in previous studies,[104] grafted polymers were found to have longer relaxation times than free chains. Others have investigated the effect of chemistry on relaxation dynamics. Recent simulations from Trazkovich *et al.*[107] considered the effect that monomer sequence can have on the dynamics of grafted polymer chains, finding that for A-B copolymers, the dynamics can be tuned to fall within the limiting cases of A or B grafted homopolymers. This tunability could be exploited to tailor the mechanical properties of nanocomposites. Molecular dynamics simulations from Ethier and Hall[128] have shown that strong polymer-nanoparticle interaction strengths can collapse the grafted layer, which may further slow relaxation dynamics. Simulations from Xu and coworkers[108] demonstrated that for grafted nanoparticles, strong polymer-nanoparticle interations resulted in enhancements in the storage and loss moduli of a nanocomposite.

Polymer dynamics are inherently tied to the glass transition temperature. Savin *et al.*[7] compared the glass transition temperature (T_g) of polystyrene when grafted to a nanoparticle surface to cleaved chains and free chains synthesized via anionic polymerization as a function of molecular weight. While the cleaved chains had values of T_g that were essentially the same as the free polymer, grafted polystyrene showed an increased T_g. For all chains, T_g decreased as molecular weight decreased. The increase in T_g for grafted chains implied more limited mobility of the chains when grafted to the SiO_2 surface, while the decrease in T_g with molecular weight highlights the role that chain ends play.[106] Dang *et al.* observed similar increases in the T_g of grafted

polystyrene.[129] Recent measurements from Torkelson *et al.*[106] are also in excellent agreement with these studies. In addition to DSC measurements, florescence spectroscopy found that T_g decreases as the distance from the nanoparticle surface increased. Finally, a detailed study comparing traditional polymer nanocomposites to SCNCs[130] found SCNCs display little physical aging – implying materials formed solely of polymer-grafted nanoparticles may more reliably retain their physical characteristics over time.

4 Conclusions and Future Outlook

Grafting polymers to nanoparticle surfaces can significantly affect their structure and dynamics. In the case of their structure, as the grafting density increases, chains become increasingly stretched due to spatial confinement by neighboring chains. For spherical nanoparticles at high grafting densities, this eventually results in a polymer brush with two regions: a concentrated polymer brush (CPB) with highly stretched chains, and a semi-dilute polymer brush (SDPB) with more ideal conformations. Both the extended DC and MWC-WZ models describe the structure well, with each theory containing relative advantages and disadvantages. In most studies, the effect of monomer chemistry, sequence, and *n*-body interactions are neglected. The inclusion of such parameters may be necessary in future studies to fully describe the structure of grafted polymer systems.

From the point of view of polymer dynamics, grafting chains to nanoparticle surfaces generally results in a slowing down of relaxation processes. However, the specific nature of how the dynamics are altered depend on factors such as the presence of a polymer matrix, relative molecular weights, grafting densities, and whether the polymers interact strongly with the nanoparticle core. Neutron spin echo (NSE) measurements of grafted polymers have resulted in a wealth of knowledge regarding the effect of interactions and spatial confinement on relaxation dynamics.

Both experimentally and theoretically, a variety of techniques have been used to probe the underlying structure and dynamics of polymers that are grafted to nanoparticles. Experimentally, these techniques range from indirect methods, such as electron microscopy[68] or dynamic light scattering,[61,67] to more direct measures such as atomic force microscopy[30] and neutron scattering.[64,69] Mean field theories reproduce the essential features of experimental observations, such as brush height[62] or approximations of single chain conformations,[64] but are not yet complete descriptions for many systems of interest. In many cases, it is a combination of these techniques that have been most successful . Nevertheless, taken together, a common picture emerges of concentrated monomers near the nanoparticle surface (*i.e.* the CPB region) that decrease in concentration as the distance from the nanoparticle surface increases. The result of this monomer concentration profile is confined chains closer to the core that are able to adopt more ideal conformations farther away. Correspondingly, the polymer dynamics are slower in the concentrated regions, and approach bulk behavior farther away from the surface.

Looking to the future, the role of factors such as interactions,[86] monomer structure, and nanoparticle shape may need to be included in extensions of the currently available models. Within the past 5 to 10 years, neutron scattering has become an invaluable tool for probing grafted polymers – especially small-angle neutron scattering (SANS) and quasi-elastic neutron scattering (QENS). A powerful concept unique to neutron scattering is the ability to contrast match different portions of the system to the surroundings through selective deuteration. With such an approach, scattering from regions of interest can be emphasized over other regions.[48,69,78,79,131] An exciting possibility for further exploring these systems may lie in using copolymer architectures[78] and contrast variation to examine polymer chains over a variety of length scales and positions along their countour. As experimental techniques and models are developed and improved upon, our insight into grafted-polymer nanoparticles is almost guaranteed to improve. With a greater understanding of these systems will come the ability to finely tune mechanical, transport, and morphological characteristics of materials based upon them, ultimately resulting in improved materials for widespread use.

Acknowledgements

MJAH acknowledges support from a National Science Foundation CAREER Award (DMR-1651002), as well as the support of the Center for High Resolution Neutron Scattering (CHRNS) at the NIST Center for Neutron Research (NCNR) by the National Science Foundation under agreement no. DMR-1508249, which has enabled many studies of grafted polymer structure and dynamics by the author using neutron scattering techniques. MJAH also thanks Boualem Hammouda (NCNR), Antonio Faraone (NCNR), and others who have contributed to these studies.

References

1 N. J. Fernandes, H. Koerner, E. P. Giannelis and R. A. Vaia, *MRS Communications*, 2013, **3**, 13–29.

2 S. K. Kumar, N. Jouault, B. Benicewicz and T. Neely, *Macromolecules*, 2013, **46**, 3199–3214.

3 S. K. Kumar, V. Ganesan and R. A. Riggleman, *The Journal of Chemical Physics*, 2017, **147**, 020901.

4 W. R. Lenart and M. J. Hore, *Nano-Structures & Nano-Objects*, 2018, **16**, 428 – 440.

5 A. Khabibullin, E. Mastan, K. Matyjaszewski and S. Zhu, in *Surface-Initiated Atom Transfer Radical Polymerization*, ed. P. Vana, Springer International Publishing, Cham, 2016, pp. 29–76.

6 C. Li, J. Han, C. Y. Ryu and B. C. Benicewicz, *Macromolecules*, 2006, **39**, 3175–3183.

7 D. A. Savin, J. Pyun, G. D. Patterson, T. Kowalewski and K. Matyjaszewski, *J. Polym. Sci. Part B: Polym. Phys.*, 2002, **40**, 2667–2676.

8 K. Ohno, T. Morinaga, K. Koh, Y. Tsujii and T. Fukuda, *Macromolecules*, 2005, **38**, 2137–2142.

9 D.-L. Zhao, X.-X. Wang, X.-W. Zeng, Q.-S. Xia and J.-T. Tang, *Journal of Alloys and Compounds*, 2009, **477**, 739 – 743.

10 P. K. Jain, X. Huang, I. H. El-Sayed and M. A. El-Sayed, *Plasmonics*, 2007, **2**, 107–118.

11 J. Gao, J. Li, S. Zhao, B. C. Benicewicz, H. Hillborg and L. S.

Schadler, *Polymer*, 2013, **54**, 3961 – 3973.
12 J. Choi, C. M. Hui, J. Pietrasik, H. Dong, K. Matyjaszewski and M. R. Bockstaller, *Soft Matter*, 2012, **8**, 4072–4082.
13 J. S. Pedersen and M. C. Gerstenberg, *Macromolecules*, 1996, **29**, 1363–1365.
14 V. Ganesan and A. Jayaraman, *Soft Matter*, 2014, **10**, 13–38.
15 P. F. Green, *Soft Matter*, 2011, **7**, 7914–7926.
16 P. F. Green, H. Oh, P. Akcora and S. K. Kumar, in *Structure and Dynamics of Polymer Nanocomposites Involving Chain-Grafted Spherical Nanoparticles*, ed. V. García Sakai, C. Alba-Simionesco and S.-H. Chen, Springer US, Boston, MA, 2012, pp. 349–366.
17 M. J. A. Hore and R. J. Composto, *Macromolecules*, 2014, **47**, 875–887.
18 M. J. A. Hore and R. J. Composto, *Current Opinion in Chemical Engineering*, 2013, **2**, 95 – 102.
19 M. Moniruzzaman and K. I. Winey, *Macromolecules*, 2006, **39**, 5194–5205.
20 S. Westenhoff and N. A. Kotov, *J. Am. Chem. Soc.*, 2002, **124**, 2448–2449.
21 B. Li and C. Y. Li, *J. Am. Chem. Soc.*, 2007, **129**, 12–13.
22 X. Yu, S. Zhong, X. Li, Y. Tu, S. Yang, R. M. Van Horn, C. Ni, D. J. Pochan, R. P. Quirk, C. Wesdemiotis, W.-B. Zhang and S. Z. D. Cheng, *J. Am. Chem. Soc.*, 2010, **132**, 16741–16744.
23 X. Yu, K. Yue, I.-F. Hsieh, Y. Li, X.-H. Dong, C. Liu, Y. Xin, H.-F. Wang, A.-C. Shi, G. R. Newkome, R.-M. Ho, E.-Q. Chen, W.-B. Zhang and S. Z. D. Cheng, *Proc. Nat. Acad. Sci.*, 2013, **110**, 10078–10083.
24 K. L. Wooley, C. J. Hawker, J. M. J. Frechet, F. Wudl, G. Srdanov, S. Shi, C. Li and M. Kao, *J. Am. Chem. Soc.*, 1993, **115**, 9836–9837.
25 X. Yu, W.-B. Zhang, K. Yue, X. Li, H. Liu, Y. Xin, C.-L. Wang, C. Wesdemiotis and S. Z. D. Cheng, *J. Am. Chem. Soc.*, 2012, **134**, 7780–7787.
26 K. Yue, C. Liu, M. Huang, J. Huang, Z. Zhou, K. Wu, H. Liu, Z. Lin, A.-C. Shi, W.-B. Zhang and S. Z. D. Cheng, *Macromolecules*, 2017, **50**, 303–314.
27 Y. Zhang and H. Zhao, *Langmuir*, 2016, **32**, 3567–3579.
28 W.-B. Zhang, X. Yu, C.-L. Wang, H.-J. Sun, I.-F. Hsieh, Y. Li, X.-H. Dong, K. Yue, R. Van Horn and S. Z. D. Cheng, *Macromolecules*, 2014, **47**, 1221–1239.
29 K. E. Geckeler and A. Hirsch, *J. Am. Chem. Soc.*, 1993, **115**, 3850–3851.
30 T. Kawauchi, J. Kumaki and E. Yashima, *J. Am. Chem. Soc.*, 2005, **127**, 9950–9951.
31 C. J. Hawker, *Macromolecules*, 1994, **27**, 4836–4837.
32 J. Kumaki, T. Kawauchi and E. Yashima, *Macromolecular Rapid Communications*, **29**, 406–411.
33 W. Kai, L. Hua, T. Dong, P. Pan, B. Zhu and Y. Inoue, *Macromolecular Chemistry and Physics*, 2008, **209**, 104–111.
34 T. Song, S. Dai, K. C. Tam, S. Y. Lee and S. H. Goh, *Langmuir*, 2003, **19**, 4798–4803.
35 Zhang, M. A. Horsch, M. H. Lamm and S. C. Glotzer, *Nano Lett.*, 2003, **3**, 1341–1346.
36 M. A. Horsch, Z. Zhang and S. C. Glotzer, *Phys. Rev. Lett.*, 2005, **95**, 056105.
37 G. Jiang, M. J. A. Hore, S. Gam and R. J. Composto, *ACS Nano*, 2012, **6**, 1578–1588.
38 S. C. Glotzer, M. A. Horsch, C. R. Iacovella, Z. Zhang, E. R. Chan and X. Zhang, *Curr. Opin. Colloid Interface Sci.*, 2005, **10**, 287 – 295.
39 C. R. Iacovella, M. A. Horsch, Z. Zhang and S. C. Glotzer, *Langmuir*, 2005, **21**, 9488–9494.
40 X. Zhang, E. R. Chan and S. C. Glotzer, *J. Chem. Phys.*, 2005, **123**, 184718.
41 A. Jayaraman and K. S. Schweizer, *J. Chem. Phys.*, 2008, **128**, 164904.
42 A. Jayaraman and K. S. Schweizer, *Langmuir*, 2008, **24**, 11119–11130.
43 X. Zhu, L. Wang, J. Lin and L. Zhang, *ACS Nano*, 2010, **4**, 4979–4988.
44 A. Chremos and J. F. Douglas, *J. Chem. Phys.*, 2015, **143**, 111104.
45 X. Lang, W. R. Lenart, J. E. P. Sun, B. Hammouda and M. J. A. Hore, *Macromolecules*, 2017, **50**, 2145–2154.
46 J. D. Nickels, J. Atkinson, E. Papp-Szabo, C. Stanley, S. O. Diallo, S. Perticaroli, B. Baylis, P. Mahon, G. Ehlers, J. Katsaras and J. R. Dutcher, *Biomacromolecules*, 2016, **17**, 735–743.
47 M. Lungova, M. Krutyeva, W. Pyckhout-Hintzen, A. Wischnewski, M. Monkenbusch, J. Allgaier, M. Ohl, M. Sharp and D. Richter, *Phys. Rev. Lett.*, 2016, **117**, 147803.
48 M. Rizk, M. Krutyeva, N. Lühmann, J. Allgaier, A. Radulescu, W. Pyckhout-Hintzen, A. Wischnewski and D. Richter, *Macromolecules*, 2017, **50**, 4733–4741.
49 A. V. Zhukhovitskiy, M. Zhong, E. G. Keeler, V. K. Michaelis, J. E. P. Sun, M. J. A. Hore, D. J. Pochan, R. G. Griffin, A. P. Willard and J. A. Johnson, *Nature Chemistry*, 2016, **8**, 33–41.
50 A. V. Zhukhovitskiy, J. Zhao, M. Zhong, E. G. Keeler, E. A. Alt, P. Teichen, R. G. Griffin, M. J. A. Hore, A. P. Willard and J. A. Johnson, *Macromolecules*, 2016, **49**, 6896–6902.
51 M. Rubinstein and R. Colby, *Polymer Physics*, Oxford University Press, 2003.
52 T. Wu, K. Efimenko and J. Genzer, *J. Am. Chem. Soc.*, 2002, **124**, 9394–9395.
53 S. A. Egorov, H.-P. Hsu, A. Milchev and K. Binder, *Soft Matter*, 2015, **11**, 2604–2616.
54 J. S. Pedersen and P. Schurtenberger, *Macromolecules*, 1996, **29**, 7602–7612.
55 E. Galati, M. Tebbe, A. Querejeta-Fernandez, H. L. Xin, O. Gang, E. B. Zhulina and E. Kumacheva, *ACS Nano*, 2017, **11**, 4995–5002.
56 R. M. Choueiri, E. Galati, H. Thérien-Aubin, A. Klinkova, E. M. Larin, A. Querejeta-Fernández, L. Han, H. L. Xin, O. Gang, E. B. Zhulina, M. Rubinstein and E. Kumacheva, *Nature*, 2016, **538**, 79–83.
57 M. Asai, D. Zhao and S. K. Kumar, *Soft Matter*, 2018, **14**, 7906–7915.

58 Y. Jiao and P. Akcora, *Macromolecules*, 2012, **45**, 3463–3470.

59 Y. Jiao and P. Akcora, *Phys. Rev. E*, 2014, **90**, 042601.

60 Daoud, M. and Cotton, J.P., *J. Phys. France*, 1982, **43**, 531–538.

61 K. Ohno, T. Morinaga, S. Takeno, Y. Tsujii and T. Fukuda, *Macromolecules*, 2007, **40**, 9143–9150.

62 C. M. Wijmans and E. B. Zhulina, *Macromolecules*, 1993, **26**, 7214–7224.

63 Y. Jiao, A. Tibbits, A. Gillman, M.-S. Hsiao, P. Buskohl, L. F. Drummy and R. A. Vaia, *Macromolecules*, 2018, **51**, 7257–7265.

64 M. J. A. Hore, J. Ford, K. Ohno, R. J. Composto and B. Hammouda, *Macromolecules*, 2013, **46**, 9341–9348.

65 P. M. Dodd and A. Jayaraman, *J. Polym. Sci. Part B: Polym. Phys.*, **50**, 694–705.

66 K. Ohno, T. Morinaga, S. Takeno, Y. Tsujii and T. Fukuda, *Macromolecules*, 2006, **39**, 1245–1249.

67 D. Dukes, Y. Li, S. Lewis, B. Benicewicz, L. Schadler and S. K. Kumar, *Macromolecules*, 2010, **43**, 1564–1570.

68 J. Choi, C. M. Hui, M. Schmitt, J. Pietrasik, S. Margel, K. Matyjazsewski and M. R. Bockstaller, *Langmuir*, 2013, **29**, 6452–6459.

69 Y. Wei, Y. Xu, A. Faraone and M. J. A. Hore, *ACS Macro Lett.*, 2018, **7**, 699–704.

70 C. Chevigny, F. Dalmas, E. Di Cola, D. Gigmes, D. Bertin, F. Boué and J. Jestin, *Macromolecules*, 2011, **44**, 122–133.

71 N. Jouault, M. K. Crawford, C. Chi, R. J. Smalley, B. Wood, J. Jestin, Y. B. Melnichenko, L. He, W. E. Guise and S. K. Kumar, *ACS Macro Letters*, 2016, **5**, 523–527.

72 A.-S. Robbes, F. Cousin, F. Meneau, F. Dalmas, R. Schweins, D. Gigmes and J. Jestin, *Macromolecules*, 2012, **45**, 9220–9231.

73 E. Buenning, J. Jestin, Y. Huang, B. C. Benicewicz, C. J. Durning and S. K. Kumar, *ACS Macro Letters*, 2018, **7**, 1051–1055.

74 M. Laradji, *J. Chem. Phys.*, 2004, **121**, 1591–1600.

75 F. Lo Verso, S. A. Egorov, A. Milchev and K. Binder, *The Journal of Chemical Physics*, 2010, **133**, 184901.

76 V. Goel, J. Pietrasik, H. Dong, J. Sharma, K. Matyjaszewski and R. Krishnamoorti, *Macromolecules*, 2011, **44**, 8129–8135.

77 S. L. Pesek, Q. Xiang, B. Hammouda and R. Verduzco, *Journal of Polymer Science Part B: Polymer Physics*, **55**, 104–111.

78 C. Mark, O. Holderer, J. Allgaier, E. Hübner, W. Pyckhout-Hintzen, M. Zamponi, A. Radulescu, A. Feoktystov, M. Monkenbusch, N. Jalarvo and D. Richter, *Phys. Rev. Lett.*, 2017, **119**, 047801.

79 A. T. Lorenzo, R. Ponnapati, T. Chatterjee and R. Krishnamoorti, *Faraday Discuss.*, 2016, **186**, 311–324.

80 J. Choi, H. Dong, K. Matyjaszewski and M. R. Bockstaller, *J. Am. Chem. Soc.*, 2010, **132**, 12537–12539.

81 M. Asai, A. Cacciuto and S. K. Kumar, *ACS Central Science*, 2018, **4**, 1179–1184.

82 H. Koerner, L. F. Drummy, B. Benicewicz, Y. Li and R. A. Vaia, *ACS Macro Letters*, 2013, **2**, 670–676.

83 P. W. Lee, S. A. Isarov, J. D. Wallat, S. K. Molugu, S. Shukla, J. E. P. Sun, J. Zhang, Y. Zheng, M. Lucius Dougherty, D. Konkolewicz, P. L. Stewart, N. F. Steinmetz, M. J. A. Hore and J. K. Pokorski, *J. Am. Chem. Soc.*, 2017, **139**, 3312–3315.

84 A. Seifpour, P. Spicer, N. Nair and A. Jayaraman, *J. Chem. Phys.*, 2010, **132**, 164901.

85 S. A. Kim and L. A. Archer, *Macromolecules*, 2014, **47**, 687–694.

86 T. B. Martin, K. I. S. Mongcopa, R. Ashkar, P. Butler, R. Krishnamoorti and A. Jayaraman, *J. Am. Chem. Soc.*, 2015, **137**, 10624–10631.

87 E. M. Sevick, *Macromolecules*, 1998, **31**, 3361–3367.

88 A. Halperin, *The European Physical Journal B - Condensed Matter and Complex Systems*, 1998, **3**, 359–364.

89 T. Hu and C. Wu, *Phys. Rev. Lett.*, 1999, **83**, 4105–4107.

90 X. Lang, A. D. Patrick, B. Hammouda and M. J. Hore, *Polymer*, 2018, **145**, 137 – 147.

91 N. J. Warren and S. P. Armes, *J. Am. Chem. Soc.*, 2014, **136**, 10174–10185.

92 S. L. Canning, G. N. Smith and S. P. Armes, *Macromolecules*, 2016, **49**, 1985–2001.

93 N. J. Warren, O. O. Mykhaylyk, A. J. Ryan, M. Williams, T. Doussineau, P. Dugourd, R. Antoine, G. Portale and S. P. Armes, *J. Am. Chem. Soc.*, 2015, **137**, 1929–1937.

94 A. Blanazs, A. J. Ryan and S. P. Armes, *Macromolecules*, 2012, **45**, 5099–5107.

95 K. I. S. Mongcopa, R. Poling-Skutvik, R. Ashkar, P. Butler and R. Krishnamoorti, *Soft Matter*, 2018, **14**, 6102–6108.

96 A. Rungta, B. Natarajan, T. Neely, D. Dukes, L. S. Schadler and B. C. Benicewicz, *Macromolecules*, 2012, **45**, 9303–9311.

97 B. Natarajan, T. Neely, A. Rungta, B. C. Benicewicz and L. S. Schadler, *Macromolecules*, 2013, **46**, 4909–4918.

98 Y. Li, L. Wang, B. Natarajan, P. Tao, B. C. Benicewicz, C. Ullal and L. S. Schadler, *RSC Adv.*, 2015, **5**, 14788–14795.

99 J. Yan, T. Kristufek, M. Schmitt, Z. Wang, G. Xie, A. Dang, C. M. Hui, J. Pietrasik, M. R. Bockstaller and K. Matyjaszewski, *Macromolecules*, 2015, **48**, 8208–8218.

100 N. Bachhar, Y. Jiao, M. Asai, P. Akcora, R. Bandyopadhyaya and S. K. Kumar, *Macromolecules*, 2017, **50**, 7730–7738.

101 K. J. Modica, T. B. Martin and A. Jayaraman, *Macromolecules*, 2017, **50**, 4854–4866.

102 P. Agarwal, S. A. Kim and L. A. Archer, *Phys. Rev. Lett.*, 2012, **109**, 258301.

103 D. Kim, S. Srivastava, S. Narayanan and L. A. Archer, *Soft Matter*, 2012, **8**, 10813–10818.

104 S. A. Kim, R. Mangal and L. A. Archer, *Macromolecules*, 2015, **48**, 6280–6293.

105 A. P. Holt, V. Bocharova, S. Cheng, A. M. Kisliuk, B. T. White, T. Saito, D. Uhrig, J. P. Mahalik, R. Kumar, A. E. Imel, T. Etampawala, H. Martin, N. Sikes, B. G. Sumpter, M. D. Dadmun and A. P. Sokolov, *ACS Nano*, 2016, **10**, 6843–6852.

106 S. Askar, L. Li and J. M. Torkelson, *Macromolecules*, 2017, **50**, 1589–1598.
107 A. J. Trazkovich, M. F. Wendt and L. M. Hall, *Soft Matter*, 2018, **14**, 5913–5921.
108 P. Xu, J. Lin and L. Zhang, *The Journal of Physical Chemistry C*, 2017, **121**, 28194–28203.
109 Y. Lin, L. Liu, D. Zhang, Y. Liu, A. Guan and G. Wu, *Soft Matter*, 2016, **12**, 8542–8553.
110 J. Mijović, H. Lee, J. Kenny and J. Mays, *Macromolecules*, 2006, **39**, 2172–2182.
111 D. Richter, M. Monkenbusch, A. Arbe and J. Colmenero, in *Neutron Spin Echo in Polymer Systems*, Springer Berlin Heidelberg, Berlin, Heidelberg, 2005, pp. 1–221.
112 G. J. Schneider, K. Nusser, L. Willner, P. Falus and D. Richter, *Macromolecules*, 2011, **44**, 5857–5860.
113 S. Srivastava, A. K. Kandar, J. K. Basu, M. K. Mukhopadhyay, L. B. Lurio, S. Narayanan and S. K. Sinha, *Phys. Rev. E*, 2009, **79**, 021408.
114 X. Frielinghaus, M. Brodeck, O. Holderer and H. Frielinghaus, *Langmuir*, 2010, **26**, 17444–17448.
115 N. Jiang, M. K. Endoh, T. Koga, T. Masui, H. Kishimoto, M. Nagao, S. K. Satija and T. Taniguchi, *ACS Macro Letters*, 2015, **4**, 838–842.
116 B. Farago, M. Monkenbusch, D. Richter, J. S. Huang, L. J. Fetters and A. P. Gast, *Phys. Rev. Lett.*, 1993, **71**, 1015–1018.
117 P. de Gennes, *Advances in Colloid and Interface Science*, 1987, **27**, 189 – 209.
118 A. Agrawal, B. M. Wenning, S. Choudhury and L. A. Archer, *Langmuir*, 2016, **32**, 8698–8708.
119 J. G. Ethier and L. M. Hall, *Macromolecules*, 2018, **51**, 9878–9889.
120 A. P. Holt, V. Bocharova, S. Cheng, A. M. Kisliuk, G. Ehlers, E. Mamontov, V. N. Novikov and A. P. Sokolov, *Phys. Rev. Materials*, 2017, **1**, 062601.
121 R. Poling-Skutvik, K. N. Olafson, S. Narayanan, L. Stingaciu, A. Faraone, J. C. Conrad and R. Krishnamoorti, *Macromolecules*, 2017, **50**, 7372–7379.
122 D. Reith, A. Milchev, P. Virnau and K. Binder, *Macromolecules*, 2012, **45**, 4381–4393.
123 F. Lo Verso, L. Yelash and K. Binder, *Macromolecules*, 2013, **46**, 4716–4722.
124 A. Chremos, A. Z. Panagiotopoulos and D. L. Koch, *J. Chem. Phys.*, 2012, **136**, 044902.
125 R. S. Hoy and G. S. Grest, *Macromolecules*, 2007, **40**, 8389–8395.
126 J. Kalb, D. Dukes, S. K. Kumar, R. S. Hoy and G. S. Grest, *Soft Matter*, 2011, **7**, 1418–1425.
127 H. Ito, T. P. Russell and G. D. Wignall, *Macromolecules*, 1987, **20**, 2213–2220.
128 J. G. Ethier and L. M. Hall, *Soft Matter*, 2018, **14**, 643–652.
129 A. Dang, C. M. Hui, R. Ferebee, J. Kubiak, T. Li, K. Matyjaszewski and M. R. Bockstaller, *Macromolecular Symposia*, **331-332**, 9–16.
130 H. Koerner, E. Opsitnick, C. A. Grabowski, L. F. Drummy, M.-S. Hsiao, J. Che, M. Pike, V. Person, M. R. Bockstaller, J. S. Meth and R. A. Vaia, *Journal of Polymer Science Part B: Polymer Physics*, **54**, 319–330.
131 K. Nusser, S. Neueder, G. J. Schneider, M. Meyer, W. Pyckhout-Hintzen, L. Willner, A. Radulescu and D. Richter, *Macromolecules*, 2010, **43**, 9837–9847.